Journal of
Materials Chemistry A

Accepted Manuscript

This is an *Accepted Manuscript*, which has been through the RSC Publishing peer review process and has been accepted for publication.

Accepted Manuscripts are published online shortly after acceptance, which is prior to technical editing, formatting and proof reading. This free service from RSC Publishing allows authors to make their results available to the community, in citable form, before publication of the edited article. This *Accepted Manuscript* will be replaced by the edited and formatted *Advance Article* as soon as this is available.

To cite this manuscript please use its permanent Digital Object Identifier (DOI®), which is identical for all formats of publication.

More information about *Accepted Manuscripts* can be found in the **Information for Authors**.

Please note that technical editing may introduce minor changes to the text and/or graphics contained in the manuscript submitted by the author(s) which may alter content, and that the standard **Terms & Conditions** and the **ethical guidelines** that apply to the journal are still applicable. In no event shall the RSC be held responsible for any errors or omissions in these *Accepted Manuscript* manuscripts or any consequences arising from the use of any information contained in them.

Graphical and textual abstract

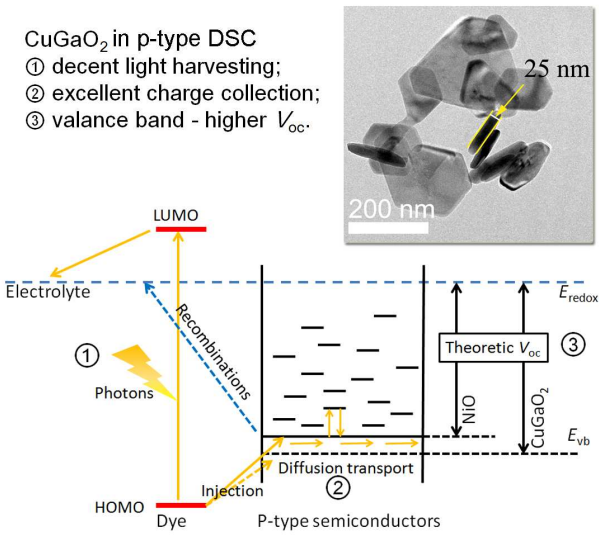

This work has demonstrate $CuGaO_2$ as efficient alternative to NiO as photocathode material in dye-sensitized solar cell. Deeper valance band position results in higher photovoltage. Critical size control of $CuGaO_2$ nanoplates and suitable film deposition technique lead to much enhanced light harvesting, in combination with excellent hole collection property, remarkable photocurrent has been achieved by $CuGaO_2$ photocathode.

Cite this: DOI: 10.1039/c0xx00000x

www.rsc.org/xxxxxx

ARTICLE TYPE

Remarkable Photocurrent of P-type Dye-sensitized Solar Cell Achieved by Size Controlled $CuGaO_2$ Nanoplates

Zhen Xu,[a] Dehua Xiong,[a] Huan Wang,[a] Wenjun Zhang,[a] Xianwei Zeng,[a] Liqun Ming, Wei Chen,*[a] Xiaobao Xu,[a] Jin Cui,[a] Mingkui Wang,*[a] Satvasheel Powar,[b] Udo Bach,[b] Yi-Bing Cheng[ab]

Received (in XXX, XXX) Xth XXXXXXXXX 20XX, Accepted Xth XXXXXXXXX 20XX
DOI: 10.1039/b000000x

In this paper, we report the successful hydrothermal synthesis of $CuGaO_2$ nanoplates with critically small size and their deposition ways to fabricate effective p-type semiconductive photocathodes in dye-sensitized solar cells (DSCs). Based on an efficient P1 dye and an iodide electrolyte, the optimal $CuGaO_2$ photocathode has achieved remarkably high photocurrent density, up to 2.05 mA cm^{-2}. To the best of our knowledge, it is the highest record achieved by nanocrystalline p-type semiconductors besides NiO. The light harvesting, charge collection in $CuGaO_2$ and NiO based DSCs have been symmetrically compared. Owing to critical size control on $CuGaO_2$ nanoplates and subsequent mechanical press for photocathode film deposition, light harvesting efficiency of $CuGaO_2$ photocathode has been for largely elevated to a comparable level to that of the NiO reference. Another noteworthy feature is the remarkably high charge collection efficiency of $CuGaO_2$ photocathode, which should be benefit from the nature of delafossite oxides with high conductivity leading to a much higher hole diffusion coefficient in DSC system. The open-circuit voltage is 199.3 mV, about twice higher than that of the NiO reference, benefiting from valance band position shifting from -5.15 eV for NiO to -5.29 eV for $CuGaO_2$ versus vacuum level.

1. Introduction

Due to continuous efforts contributed by world-wide researchers during the past 20 years, low-cost dye-sensitized solar cell (DSC) with competitive performance now is regarded as one of the most promising next generation photovoltaic technologies.[1-5] Recently reported new efficiency record is 12.3%, achieved by introducing a porphyrin dye with broad light harvesting range.[6] To date, all of the reported high performance DSCs are based on dye-sensitized n-type nanocrystalline semiconductors, such as TiO_2, ZnO, *etc.*,[6,7] which we can call n-type DSCs. The research on dye sensitized p-type semiconductors, called p-type DSCs, lags much behind. The best p-type DSCs are with only 0.41-1.30% in efficiency, achieved by a well designed push-pull dye (PMI-6TTPA-TPA) in conjunction with NiO nanoparticles.[8,9] Limitations of current p-type DSCs arise from lack of ideal p-type semiconductors as photocathodes and efficient dyes compatible for them. Nonetheless, the p-n tandem design of DSC holds great potential in the future. By positioning two different dyes on physically separated n-type photoanode and p-type photocathode, p-n tandem DSC in principle can break through the theoretical efficiency limit for a single junction solar cell. The light utilization range can be effectively broadened. Open-circuit photovoltage (V_{oc}) of the serially connected tandem cell is accordingly improved in comparison to each single cell.[8]

Until now, NiO nanoparticles have been the most commonly used as the photocathode material. Within the limited binary oxides with p-type semiconductivity in nature, NiO is a compromised choice because of its wide band gap (3.6 eV) and high chemical stability. However, its drawbacks are also evident: (1) its valance band (E_{vb}, -5.1 - -5.2 eV versus vacuum level) is too close to the redox potential of iodide electrolyte, resulting in small V_{oc} of p-type DSCs and therefore limited V_{oc} enhancement in p-n tandem DSCs;[10] (2) the intrinsic light absorption by NiO owing to d-d transition which does not contribute to the cathodic photocurrent, largely hinders effective light harvesting by the sensitizers. In the best NiO based DSC, the effective light harvesting efficiency (*LHE*) by the adsorbed dye molecules was reported with only ~60%; the other part was wasted;[8] (3) hole transport is questionable in the reported mesoporous NiO films: the carrier diffusion coefficients tested by transient method or other electrochemical methods are in the magnitudes of 10^{-8}-10^{-7} $cm^2\ s^{-1}$, which are typically two-three orders lower than electrons in mesoporous TiO_2 films.[11] The consequence is the limited charge collection efficiency and low fill factor (0.3-0.4) of NiO based p-type DSCs.[12]

Therefore, it is crucial to find alternative p-type semiconductors to NiO with better optical transparency, more negative E_{vb} (versus vacuum level) and higher hole mobility.[11] Luckily, some delafossite ABO_2 (A = Cu, Ag; B = Al, Ga, In, Fe, Cr, Y, Sc, *etc*.) materials just meet all of these demands simultaneously, which have gained increased attention for the applications in p-type DSCs.[13-18] Delafossite ABO_2 materials in

the research history were designed as p-type transparent conductive oxides (TCOs) for thin film photoelectronics applications, as the counterparts of indium doped tin oxide (ITO), a well-known n-type TCO.[19, 20] Dense thin films made of p-type ABO_2 materials generally feature tunable E_{vb} (-5.2 - -5.5 eV versus vacuum level), high hole conductivity (10^{-2}-10^{2} S cm^{-1}), wide band gaps (3.0-3.6 eV) and decent optical transparency (50-80%).[14-18] More negative E_{vb} versus vacuum than that of NiO allows generating higher V_{oc} of the corresponding solar cells, which have been proved in recently published literatures.[14-18] Transparency benefiting light harvesting has also been demonstrated in our recent papers on nanocrystalline $CuCrO_2$ and Mg doped $CuCrO_2$ based p-type DSCs.[17,18] But $CuCrO_2$ derivates still present certain colors.[21] Colorless delafossite oxides, such as $CuAlO_2$, $CuGaO_2$ which have full d-orbitals of B site elements, are suggested to be more advantageous for p-type DSC applications. Unlucky, to synthesize nanocrystalline $CuAlO_2$ or $CuGaO_2$ with small enough sizes still remains as great challenge.[14] In 2012, Wu YY *et al*.[15] and Fabrice Odobel *et al*.[16] reported their independent research on p-type DSCs based on $CuGaO_2$ nanoplates, with the size of 200-400 nm in nanoplate diameter and the smallest 45 nm in nanoplate thickness. Their reported short circuit photocurrent densities (J_{sc}, 0.38 and 0.29 mA cm^{-2}, respectively) were greatly restricted by the materials' small specific surfaces, which were detected to be with 3-5 fold differences to the NiO nanoparticles references.[15, 16]

In this work, we paid more effort to optimizing the synthesis of $CuGaO_2$ nanoplates with more competitive size (~150 nm in average diameter, ~25 nm in average thickness), and developed a better technique to fabricate the mesoporous $CuGaO_2$ film with respect to the specific nanoplate morphology. Indeed, by using P1 dye and iodine electrolyte, p-type DSC based on $CuGaO_2$ nanoplates has achieved a remarkable J_{sc} of 2.05 mA cm^{-2}, which is more competitive to the widely reported NiO photocathodes and is evidently higher than our previous records achieved by $CuCrO_2$ derivates based p-type DSCs (1.2-1.5 mA cm^{-2}, based on the same dye and electrolyte).[17] Besides, in this paper, we have systematically evaluated the light harvesting and hole collection of $CuGaO_2$ based DSC with NiO based DSC as the reference. All these have important referential significance for further improving the properties of nanocrystalline $CuGaO_2$ as ideal photocathode materials and achieving high performance of p-type DSCs.

2. Experimental Section

2.1 Synthesis of $CuGaO_2$ nanoplates

All chemicals used were of analytical reagent grade. $Ga(NO_3)_3{\cdot}xH_2O$ (99.9% in purity) was purchased from Sigma-Aldrich. $Cu(NO_3)_2{\cdot}3H_2O$, KOH, ethylene glycol (EG) and poly ethylene glycol (PEG, Mn = 20000) were purchased from Aladdin reagent company, Shanghai, China.

The hydrothermal synthesis procedure of $CuGaO_2$ was modified from the literature.[22] Typically, 0.6 mmol $Ga(NO_3)_3{\cdot}xH_2O$ and 0.6mmol $Cu(NO_3)_2{\cdot}3H_2O$ were dissolved in 3.6 ml deionized water. 3ml EG and 0.1 g PEG 20000 were subsequently added. The temperature of the solution was controlled at 5, 25 or 50 °C in ice bath or water bath. Then, 6 ml of 0.5 M KOH solution was dropwise added to adjust the pH value of the hydrothermal precursor to be 8.0. The hydrothermal precursor was then transferred into an 18 ml Teflon-lined autoclave and kept at 190 °C in an oven for 56 hours. The obtained precipitate with light yellow color was washed with diluted ammonia aqueous solution and dilute HNO_3 solution in sequence for several times, followed by washing with distilled water and ethanol to obtain phase pure $CuGaO_2$. Finally, the $CuGaO_2$ sample was stored in absolute alcohol solution for further use.

2.2 Preparation of $CuGaO_2$ films and DSSCs

$CuGaO_2$ sample dispersed in ethanol as "nano-ink" for spray deposition of the films. An air spray gun was used. Before deposition, the edges of FTO glass substrates (8 Ω $square^{-1}$, Nippon Sheet Glass, Japan) were covered by tapes to determine the geometrical shape of the deposited films. The as-deposited films were dried at 125 °C for 30 minutes, and then were pressed mechanically at the pressure of 100 MPa. Film thickness was tuned by the deposition time and the solid content in the "nano-ink". As a controlled experiment, some films were prepared without mechanical press, according to the previous literature.[15] After that, the films deposited by both of the preparation techniques were sintered on a hotplate at 350 °C for 30 minutes in air.

After the films were cooled to 80 °C, they were immersed into 0.3 mM acetonitrile solution of P1 dye and kept at room temperature for 18 hours for sensitizer uptake. Catalytic counter electrodes were prepared by pyrolysis of H_2PtCl_6 solution (120 μg cm^{-2}) on FTO glasses, using a hot-wind gun being set at 400 °C for 20 minutes. The dye sensitized $CuGaO_2$ photocathodes were sandwiched together with the platinized counter electrodes, and sealed with a hot melt polymer gasket (25 μm, Surlyn). The 1.0M LiI/0.1M I_2/acetonitrile electrolyte was injected into the cell through a drilled hole via vacuum back-filling technique.

2.3 Characterization

Material Characterizations: The $CuGaO_2$ crystal phase was identified by X-ray powder diffraction (XRD, X'Pert PRO, Cu Kα radiation, Panalytical B. V.). The morphology of $CuGaO_2$ was observed using a field emission scanning electron microscope (FE-SEM, FEI-Sirion 200, FEI), and a transmission electron microscope (TEM, Tecnai G_2 20). The $CuGaO_2$ film thickness was measured by a profilometer (Dektak 150, Veeco Instruments Inc.). UV-vis-NIR spectra of the films were recorded on a Perkin-Elmer UV/Vis spectrophotometer (Lambda 950). The valance band edges of $CuGaO_2$ and NiO were analyzed by photoelectron spectroscopy in air (PESA), using a Riken-Keiki AC-2.

Photovoltaic Characterizations: a 450W xenon light source solar simulator (Oriel, model 9119) with AM 1.5G filter (Oriel, model 91192) was used to give an irradiance of 100 mW cm^{-2}. Light intensity was calibrated with a standard silicon reference cell. The current-voltage characteristics of the cell under these conditions were obtained by applying external potential bias to the cell and measuring the generated photocurrent with a Keithley

model 2400 digital source meter (Keithley, USA). The active area for solar cell measurement was determined by a 4 × 4 mm^2 mask, to prevent scattering light. A similar data acquisition system was used to control the IPCE measurement. A white light bias (1% sunlight intensity) was applied onto the sample during the IPCE measurements with ac model (10 Hz).

Determination of apparent hole diffusion coefficients and recombination hole lifetime: Transient photovoltage/photocurrent decay measurements were employed to determine hole lifetime and hole diffusion coefficients in p-type DSCs. They were done on a home-made photo-electrochemical system. A white light bias on the sample was generated from an array of diodes. Red light pulse diodes (0.05 s square pulse width, 100 ns rise and fall time) controlled by a fast solid-state switch were used as the perturbation source. The voltage dynamics were recorded on a PC-interfaced Keithley 2602A source meter with a 100 μs response time. The perturbation light source was set to a suitably low level in order for the voltage decay kinetics to be monoexponential. By varying the white light bias intensity, the recombination rate constant and hole diffusion rate constant could be estimated over a range of applied biases.

3 Results and Discussion

3.1 Size control of $CuGaO_2$ nanoplates

The optimal $CuGaO_2$ sample with the smallest size was synthesized by controlling the reaction temperature of the hydrothermal precursor to be 5 °C. Phase purity of the as-prepared $CuGaO_2$ sample is confirmed by the X-Ray Diffraction (XRD) pattern shown in Fig. 1a, which matches well with the standard JCPDF card (No. 41-0255). Shown in Fig. 1b is the optical image of the $CuGaO_2$ film with 1 μm thickness prepared by spray deposition. It looks semitransparent with light yellow color. For DSC application, such optical appearance is thought to be superior to NiO and $CuCrO_2$. The latter two are with some greyish-green color which will compete with effective light absorption by the dye sensitizer adsorbing on them. The scanning electron microscope (SEM) (Fig. 1c) and transmission electron microscope (TEM) (Fig. 1d) images show that the obtained nanoparticles are with the hexagonal nanoplate morphology. From microscopy observations, the average diameter of nanoplates is about 100-200 nm and the average thickness is roughly 20-30 nm. The double ends of nanoplates could be indentified to be {001} planes of delafossite structure.[15] Therefore, we could use the (003) and (006) peaks of the XRD pattern (Fig. 1a) to calculate the nanoplate thickness on the basis of the well-known Scherrer equation.[23] The calculated result is 25.7 nm, consistent with TEM observation. In comparison to the literature reported size,[15,16] the smallest of which was 45 nm × 200-400 nm, the surface area for our optimal sample should be much higher, which may lead to critical change on the dye-adsorbing amounts and accordingly the solar cell performance. Actually, when referring to the size optimization of TiO_2 nanoparticles in n-type DSCs, slightly tuning the size on the nanometer scale, the cell performance could be largely changed.[24, 25]

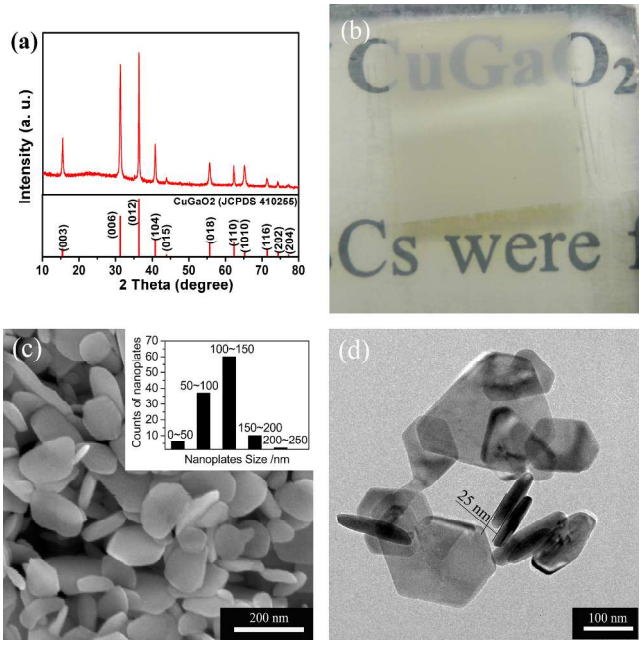

Fig. 1 Characterization of the optimal $CuGaO_2$ nanoplates: (a) XRD pattern, (b) digital photo of the as-deposited $CuGaO_2$ film on FTO glass substrate, with the thickness of 1 μm, (c) SEM image and (d) TEM image. The inset in (c) shows the size distribution of $CuGaO_2$ nanoplates, obtained by counting the SEM image.

Shown in the right side of Fig. 2 are SEM images of three $CuGaO_2$ samples synthesized from the hydrothermal precursors prepared at different temperatures. Note that other parameters were controlled to be the same. From Fig. 2e-g, it is easily known that the precursor temperature has a strong impact on the size of the finally-obtained $CuGaO_2$ nanoplates. As the temperature increases from 5 °C, 25 °C to 50 °C, the nanoplates gradually grows from 25 nm × 100-200 nm (Fig. 2e), 50 nm × 200-400 nm (Fig. 2f) to microns (Fig. 2g). The temperature control is the primary difference of this work from the literatures for $CuGaO_2$ synthesis,[15, 16, 22] and should be responsible for the smaller size of the optimal $CuGaO_2$ nanoplates in this work than the literatures. The BET surface areas for the "25 nm × 100-200 nm" and "50 nm × 200-400 nm" $CuGaO_2$ nanoplates are tested to be 37.9 $m^2 g^{-1}$ and 17.6 $m^2 g^{-1}$, respectively. Such about twice difference on BET surface area is consistent with calculation (Fig. S1) and is suggested to be the main reason responsible for their *LHE* difference as described later.

Why does the hydrothermal precursor temperature play such a critical role in determining the size of $CuGaO_2$ nanoplates? In order to answer this question, we resort to characterizing the structure difference of the solid intermediates obtained from different hydrothermal precursors and monitoring the morphology/structure evolutions of the intermediates in the early stage of hydrothermal reaction (for example, after hydrothermal treatment at 190 °C for 1 hour, 5 hours and 10 hours). Shown in the left side of Fig. 2 are SEM images of the intermediates before hydrothermal treatment, as the temperature increases, the morphology varies from nanosized fibrous (Fig. 2a,b) to submicron sheet-like (Fig. 2c). Digital photos of the three different precursors are shown as the insets in Fig. 2a-c. It can be

Cite this: DOI: 10.1039/c0xx00000x

www.rsc.org/xxxxxx

ARTICLE TYPE

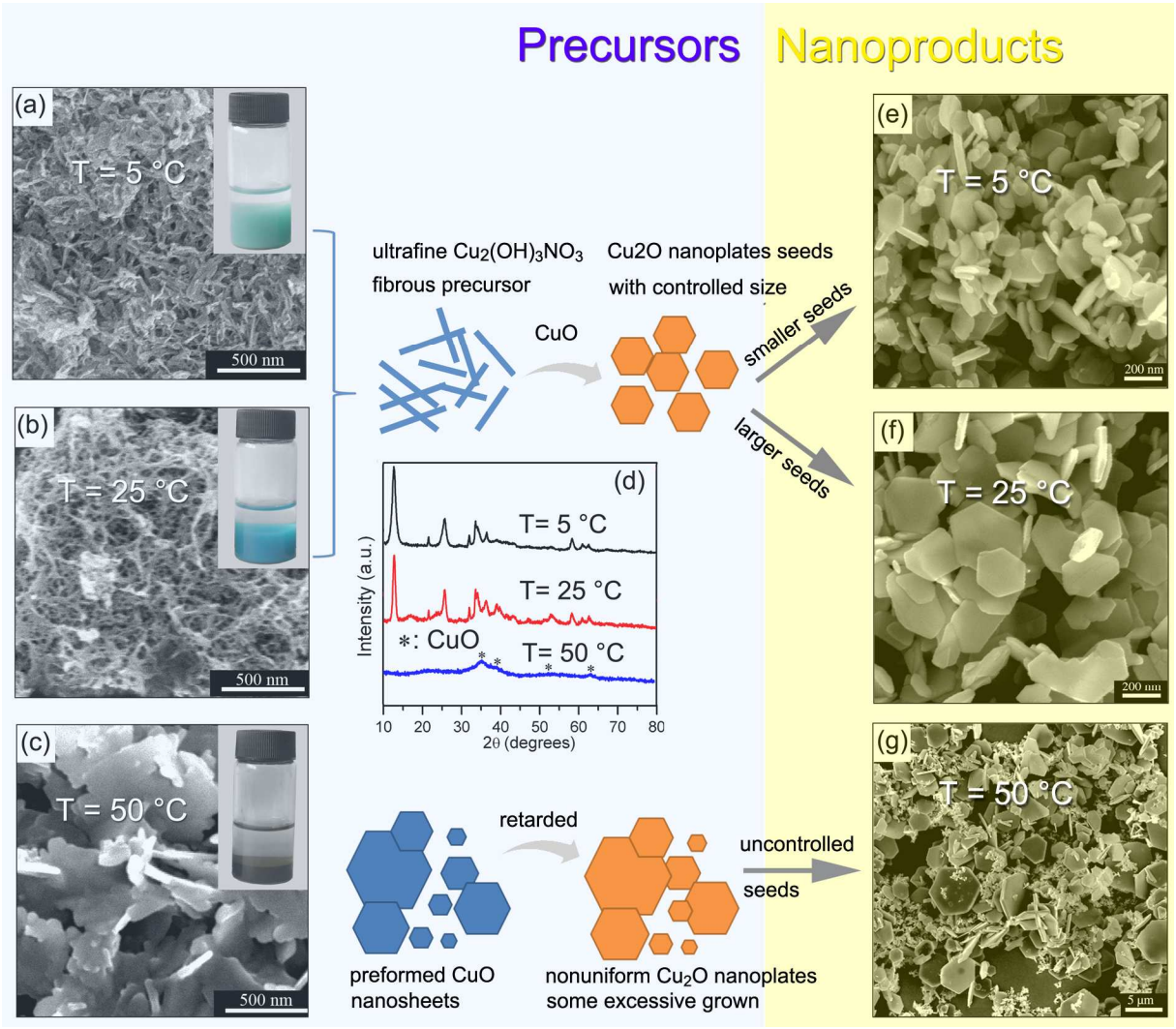

Fig. 2 SEM images of the intermediates in hydrothermal precursors at different temperatures: (a) 5 °C, (b) 25 °C, (c) 50 °C. The insets in (a-c) are the digital photos of the three different precursors. (d) XRD pattern of the three intermediates. SEM images of three $CuGaO_2$ samples synthesized from the hydrothermal precursors at different temperatures (e) 5 °C, (f) 25 °C, (g) 50 °C

clearly observed that the color of the intermediates at the bottom of the vials varies from light blue (5 °C precursor), dark blue (25 °C precursor) to dark brownish red (50 °C precursor), implying there are structural difference among them. XRD characterization (Fig. 2d) reveals that the fibrous intermediates in the 5 °C and 25 °C precursors are mostly with gerhardtite-$Cu_2(OH)_3NO_3$ crystal phase; besides, $Cu_2(OH)_3NO_3$ crystal in the 25 °C precursor is relatively larger than in the 5 °C precursor, as reflected by their difference on full width at half maximum of their XRD patterns; the sheet-like intermediate in the 50 °C precursor is mostly with CuO crystal phase. These intermediates after hydrothermal treatment for 1 h, 5 h and 10 h were found to gradually convert into Cu_2O and subsequent $CuGaO_2$ (Fig. S2). During such phase transition process, the Ga source always remains as ions dissolved in the solution. On the basis of the similar nanoplate morphologies of Cu_2O and $CuGaO_2$ (Fig. S3), it is believed that the Cu_2O nanoplates act as the crystal seeds, accepting the insertion of Ga^{3+} into their lattice and leading to $CuGaO_2$ nanoplates formation. So, it is critical to control the growth of Cu_2O seeds for controlling the $CuGaO_2$ nanoproduct's morphology. For the 50 °C precursor, the preformed CuO nanosheets might retard the CuO to Cu_2O phase transition during the first several hours of hydrothermal treatment, which prolonged the formation time of Cu_2O and resulted in nonuniform Cu_2O seeds with some excessively grown (Fig. S3c,d). That can explain why the $CuGaO_2$ product in Fig. 2g is so large and nonuniform. It is suggested that at the decreased temperatures (5 °C and 25 °C), the hydrolysis and condensation reactions of

Cite this: DOI: 10.1039/c0xx00000x

www.rsc.org/xxxxxx

ARTICLE TYPE

Table 1 Performance of DSCs based on different photocathodes

Samples	Size	Film preparation method	Thickness / μm	V_{oc} / mV	J_{sc} / mA cm^{-2}	Fill factor	Efficiency / %
$CuGaO_2$	25 nm × 100-200 nm	Pressed, binder free	1.6	216.8	0.81	41.6	0.073
$CuGaO_2$	25 nm × 100-200 nm	Pressed, binder free	2.9	199.3	2.05	44.5	0.182
$CuGaO_2$	25 nm × 100-200 nm	Pressed, binder free	4.0	185.8	1.32	41.1	0.101
$CuGaO_2$	50 nm × 200-400 nm	Pressed, binder free	3.0	177.4	0.67	42.9	0.051
$CuGaO_2$	25 nm × 100-200 nm	Binder, without press	2.2	212.5	0.59	44.1	0.055
$CuGaO_2$	25 nm × 100-200 nm	Binder, without press	3.0	180.1	1.09	45.7	0.090
$CuGaO_2$	25 nm × 100-200 nm	Binder, without press	4.5	188.0	0.64	43.0	0.065
NiO	20 nm	Binder, calcined	2.4	108.4	1.89	35.0	0.072

Cu^{2+} ions in weak alkaline condition were suppressed. The Cu source was in the form of $Cu_2(OH)_3NO_3$ rather not CuO. During the subsequent hydrothermal treatment, the phase transition from $Cu_2(OH)_3NO_3$ to CuO, and to Cu_2O could occur within a relatively shorter time. Therefore, the Cu_2O seeds were more uniform and with better controlled size (Fig. S3a,b), which leaded to the formation of ultrasmall $CuGaO_2$ nanoplates. Furthermore, it might be due to in the 5 °C precursor, the $Cu_2(OH)_3NO_3$ was with higher degree of dispersion and smaller size, which converted into smaller Cu_2O seeds than that in the 25°C precursor, the $CuGaO_2$ nanoplates in Fig. 2e are smaller than in Fig. 2f.

3.2 Performance optimization of $CuGaO_2$ based DSCs

The optimal $CuGaO_2$ nanoplates with the size of about 25 nm × 100-200 nm were then processed into uniform films for p-type DSC applications. In order to optimize film thickness with respect to solar cell performance, the $CuGaO_2$ photocathodes with the thicknesses of 1.6 μm, 2.9 μm and 4.0 μm have been compared. For each thickness, three cells have been characterized in parallel in order to get the reproducible results. These films were all treated by mechanical press and post sintering at 350 °C in air. The performance results are summarized in Table 1. It can be found that, in general, V_{oc} decreases monotonically from 216.8 mV to 185.8 mV as the film becomes thicker, while J_{sc} peaks at the middle thickness of 2.9 μm with the value of 2.05 mA cm^{-2}. In total, the efficiency of $CuGaO_2$ based DSCs gets saturated at 2.9 μm with the value of 0.182%. In comparison to the reported $CuGaO_2$ based DSCs,[15, 16] noteworthy is the 5-6 folds improved J_{sc} in this work.

In order to clarify how critical the size of $CuGaO_2$ nanoplates leads to such dramatically improved J_{sc}, the photovoltaic performance of $CuGaO_2$ nanoplates with the size of about 50 nm × 200-400 nm (prepared from 25 °C precursor) has also been checked in a controlled experiment (Table 1). J_{sc} was tested to be only 0.67 mA cm^{-2} for the relatively larger nanoplates. Nearly three folds lower J_{sc} should be mostly ascribed to the poor *LHE* of the larger sample, the maximum of which at 510 nm wavelength was tested to be 21% versus 55% for the smaller sample (Fig. 3a).

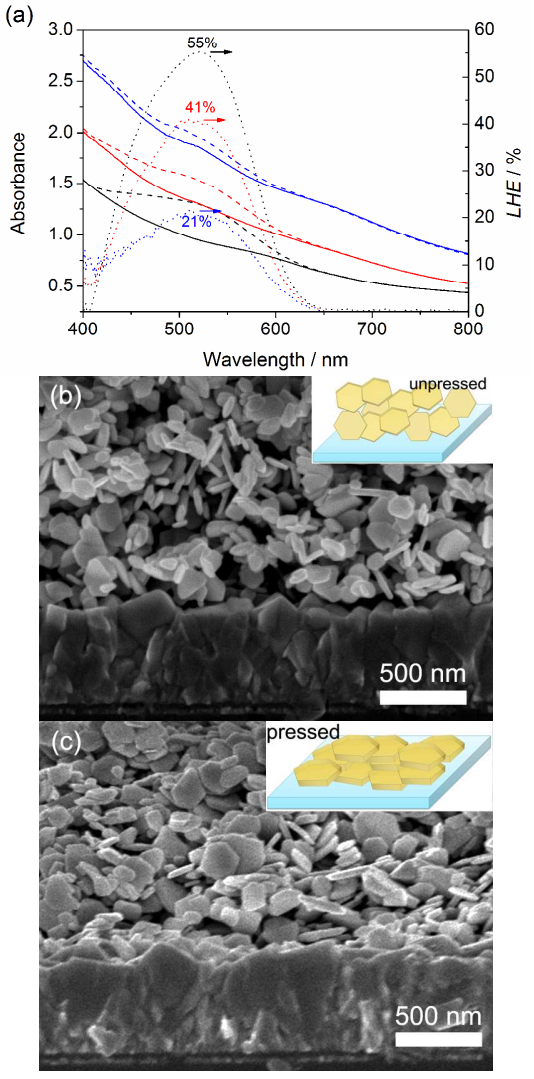

Fig. 3 (a) Comparison on effective *LHE*s for the films made of 25 nm × 100-200 nm $CuGaO_2$ nanoplates before (red dot line) and after (black dot line) mechanical press, and 50 nm × 200-400 nm nanoplates after press (blue dot line). The *LHE*s are calculated from the absorbance difference between the dyed (dash lines) and undyed (solid lines) films. Cross sectional SEM images of the $CuGaO_2$ films prepared by (b) calcination, without press, (c) mechanical press.

Cite this: DOI: 10.1039/c0xx00000x

www.rsc.org/xxxxxx

ARTICLE TYPE

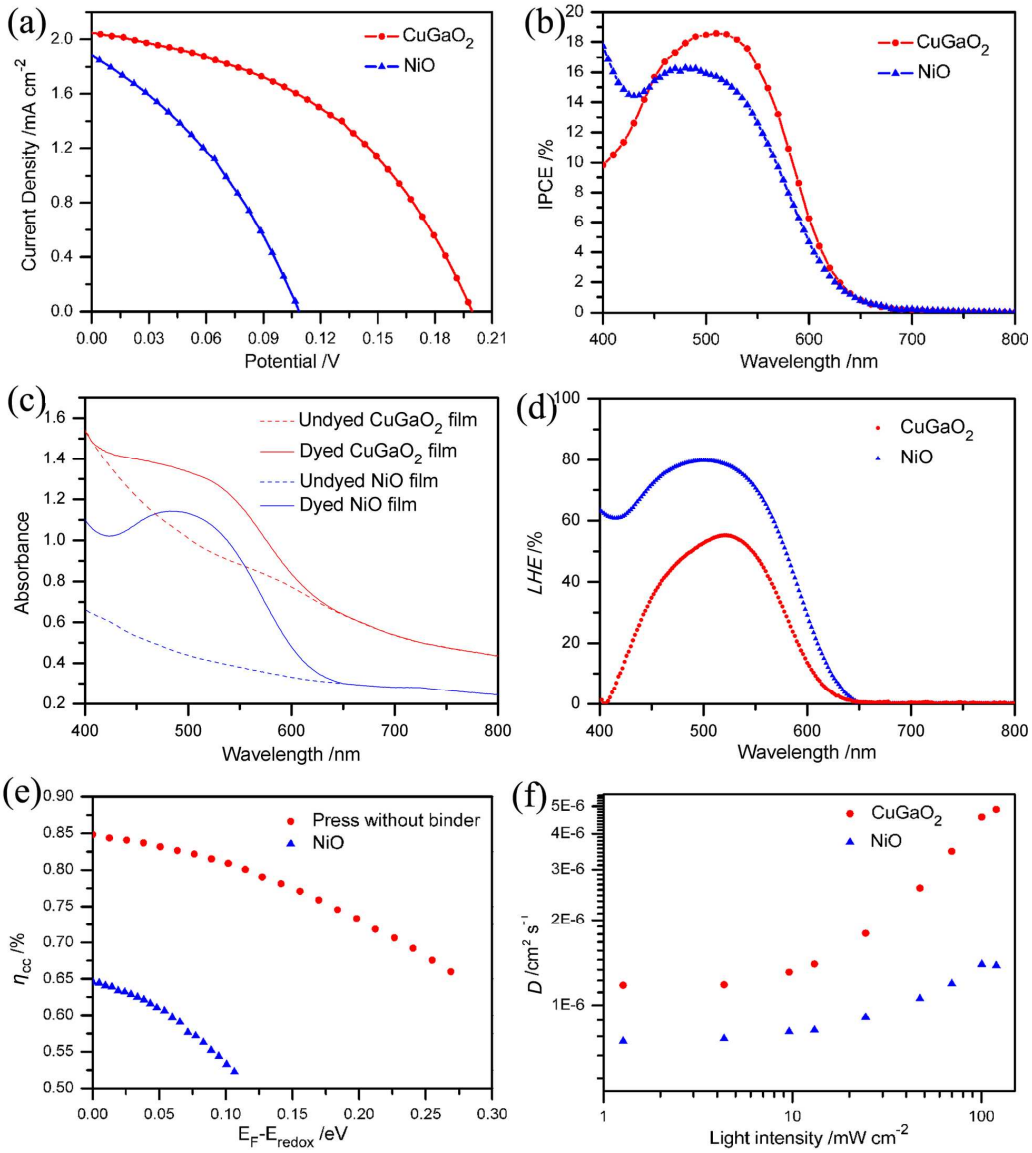

Fig. 4 Photocurrent density-voltage characteristic curves, (b) IPCE spectra of $CuGaO_2$ and NiO based solar cells; (c) diffuse reflectance absorption spectra of the undyed (bare) and dyed $CuGaO_2$ and NiO films; (d) the calculated light harvesting efficiency (*LHE*), (e) charge collection efficiency (η_{cc}), and (f) hole diffusion coefficient (D) for the two compared solar cells.

Besides size optimization, another notable improvement in this work is the film preparation way, which has been demonstrated to be also important for the J_{sc} enhancement. The optimal films in this work were prepared from binder free paste (or called "nano-ink"), by spray deposition, and then treated by mechanical press. This mechanical press strategy was simply copied from the preparation of TiO_2 nanoparticles films on conductive plastic substrates in efficient flexible DSCs, in order to promote inter-nanoparticles contacts at relatively low temperature.[26] As shown in Table 1, the performance of p-type DSCs based on $CuGaO_2$ films prepared according to the literature[15] without mechanical press were much worse than the mechanical pressed samples. The optimal J_{sc} for the unpressed films was only 1.09 mA cm^{-2}. The film morphologies prepared by two different ways are shown in Fig. 3b and 3c. It is easy to find that, for film prepared by the literature way, the nanoplates without mechanical press are randomly assembled, resulting in very hollow film structure. That would waste a lot of inner space within the film, resulting in poor specific surface area per thickness.[27-29] By mechanical press technique, the film's structure becomes closely packed, which can

be reflected by their narrower pore size distribution (Fig. S4). The maximum *LHEs* for two films at the same thickness of 3.0 μm before and after mechanical press were tested to be 41% and 55%, respectively (Fig. 3a). The BET surface area for the pressed sample was tested to be 30.7 m^2 g^{-1}, about 20% smaller than that of the unpressed sample (37.9 m^2 g^{-1}). Such result seems to be contradictory to the *LHE* improvement. However, if considering the compression ratio of 1.5-1.7 associated with mechanical press, it is not surprise to see the *LHE* for the pressed sample is even higher. That is because the dye loading content is more related to the roughness factor rather not the BET surface area. Roughness factor is determined by the BET surface area of $CuGaO_2$ multiplying by the $CuGaO_2$ weight per thickness. The enhancement on *LHE* should be one important reason responsible for the J_{sc} improvement for the pressed film than the unpressed one. Furthermore, the thermal stability of $CuGaO_2$ is not so good, which cannot stand for air sintering at the temperature higher than 350 °C.[15, 16] Therefore, the literatures ways involving organic binder in the pastes for $CuGaO_2$ film preparation are not recommended,[15, 16] because at such a low sintering temperature, the organics may not be totally evaporated way or burned out; such residues are generally considered not good for the solar cell performance.

3.3 Comparison between $CuGaO_2$ and NiO in DSCs

In this paper, we have also compared the performance of the optimal $CuGaO_2$ based DSC with respect to the NiO reference cell. NiO nanoparticles (20 nm in size, Inframat Advanced Materials, USA) were processed into films by screen-printing according to the literature.[8] The results are shown in Fig. 4a and Table 1. It is found that in comparison to the NiO reference cell, J_{sc} of the $CuGaO_2$ based DSC is a little bit higher (2.05 mA cm^{-2} versus 1.89 mA cm^{-2}), V_{oc} is dramatically increased from 108.4 mV to 199.3 mV and fill factor is also increased from 0.35 to 0.45. In total, the efficiency of the $CuGaO_2$ based DSC is accordingly increased by ~2.5 times (0.182% versus 0.072%).

Regarding to the J_{sc} difference between the two compared cells,their IPCE difference shown in Fig. 4b can just explain. It is found that the incident photo-to-current conversion efficiency (IPCE) maximum at 510 nm for the $CuGaO_2$ based DSC is about 18.8%, a little bit higher than that of the NiO reference (16.7%). It is known that IPCE is determined by the following three factors, including *LHE*, injection efficiency from dye to semiconductor (Φ_{inj}), and charge collection efficiency (η_{cc}), according to the equation of IPCE = $LHE \times \Phi_{inj} \times \eta_{cc}$.[30] Which factor dominates the IPCE difference for the two compared cells? The answer to this question will be instructive for further improving $CuGaO_2$ based p-type DSC's performance in the future.

First, their effective *LHE*s by the P1 dye have been compared. The effects of light absorption and light scattering arising from the scaffold mesoporous films have been avoided, by using the diffuse reflectance absorption spectra of the bare films as the references (Fig. 4c). The calculated *LHE*s are shown in Fig. 4d. The results reflect that the maximum *LHE* at 520 nm for the $CuGaO_2$ film is 55%, while the maximum *LHE* at 500 nm for the NiO reference film is 80%. Such *LHE* difference basically reflects the difference on dye adsorbing amount between the two compared films. Though, *LHE* for the 2.9 μm-thick $CuGaO_2$ film is still inferior to that of 2.3 μm-thick NiO film, in comparison to the reported 3-5 fold difference on *LHE*s in the literatures,[15,16] the *LHE* gap is dramatically narrowed through our effort on critically optimizing the size of $CuGaO_2$ nanoplates and improving the film preparation way.

Second, the η_{cc} difference between the two compared cells has been evaluated by the transient photovoltage/photocurrent decay techniques. The results are shown in Fig. 4e. It can be found that at the short circuit condition, η_{cc} for the $CuGaO_2$ based DSC is 85%, which is much higher than that of the NiO reference cell with the data of 65%. The improved η_{cc} is mostly ascribed to the enhanced hole diffusion coefficient (D) of the $CuGaO_2$ photocathode than the NiO reference (Fig. 4f, 1.9-5.0×10^{-6} cm^2 s^{-1} versus 0.7-1.3×10^{-6} cm^2 s^{-1}). When referring to our previous studies on $CuCrO_2$ and Mg doped $CuCrO_2$ based p-type DSCs,[17, 18] it can be found that higher hole diffusion coefficient is a common feature for all of these delafossite oxides based photocathodes, which we believe is benefit from the nature of delafossite oxides with high p-type conductivity.[31]

By these systematical comparisons, it can be concluded that the superior η_{cc} of the $CuGaO_2$ photocathode should be the dominated reason for its higher J_{sc} than that of the NiO reference, which compensate its drawback on *LHE*. It is also known that to improve the decent *LHE* from currently 55% to more than 80% should be of critical importance for further increasing J_{sc} of the $CuGaO_2$ based DSC in the future. The next step is to further decrease the thickness of $CuGaO_2$ nanoplates to be about 10-20 nm. By doing so, higher specific surface area per thickness and also better optical transparency of the $CuGaO_2$ based photocathode could be expected.

Regarding to the dramatic V_{oc} improvement of the $CuGaO_2$ based DSC than that of the NiO reference cell, it can be ascribed to the negative shift of valance band of $CuGaO_2$ than NiO. We here employed the photoelectron spectroscopy with very high resolution to measure the valance band positions of NiO and $CuGaO_2$ in the air. The results are shown in Fig. 5. It could be found that the ionization potentials for $CuGaO_2$ nanoplates and NiO nanoparticles are 5.29 eV and 5.15 eV respectively. The ionization potential is defined as the energy difference between valence band maximum and the vacuum level. Therefore, it is known that the valance band positions for $CuGaO_2$ nanoplates and NiO nanoparticles are -5.29 eV and -5.15 eV versus vacuum. The positions are consistent well with the literature reported flat band potentials measured in an electrochemical environment by Mott-Schottky method.[16] The as-measured flat band potentials of NiO and $CuGaO_2$ are 0.33 and 0.49 versus SCE, which after converting into versus vacuum level are -5.075 and -5.235 eV, respectively. More negative valance band of semiconductive photocathode corresponds to larger energy gap with respect to the redox potential of the electrolyte, which will result in higher V_{oc} of p-type DSC. The valance band difference (0.14 eV) between $CuGaO_2$ and NiO could almost explain the V_{oc} difference between the two compared solar cells (199.3 mV versus 108.4 mV).

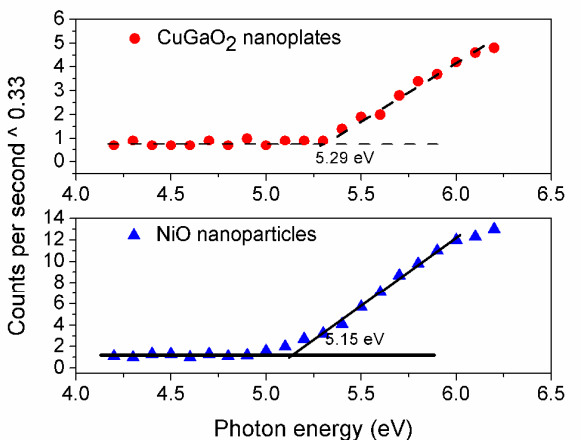

Fig. 5 The ionization potentials of $CuGaO_2$ nanoplates and NiO nanoparticles

4. Conclusion

In conclusion, we have captured the key factor, *i.e.*, the temperature of the hydrothermal precursor to improve the synthesis of $CuGaO_2$ nanoplates with critically smaller size. The *LHE* of the $CuGaO_2$ photocathode is according much improved in comparison to previous reports,[15, 16] especially when the film is prepared by a mechanical press method, which is developed with respect to the specific two-dimensional morphology of nanoplates. The J_{sc} of the optimal $CuGaO_2$ based DSC sensitized by the P1 dye reaches 2.05 mA cm^{-2}, which is the best among kinds of delafossite oxides based photocathodes we have tried before,[17, 18] and is also significantly improved in comparison to the literatures reported data.[14-16] When taken into comparison with the NiO nanoparticles based photocathode, the charge collection efficiency of $CuGaO_2$ based photocathode is evidently higher owning to the higher hole diffusion coefficient. J_{sc} is accordingly a little bit higher for the $CuGaO_2$ photocathode. V_{oc} of the $CuGaO_2$ photocathode is nearly doubled in comparison to the NiO reference, which is confirmed to be due to more negative valance band edge position of $CuGaO_2$. The decent solar cell performance of p-type DSC achieved in this work strongly suggest $CuGaO_2$ might be the right choice alternative to traditional NiO, worthy for further optimization as ideal photocathode material in p-type DSC. It is believed that further decrease on the thickness of $CuGaO_2$ nanoplates holds the key for further improving the related solar cell's performance. The related work is in progress in our laboratory.

Acknowledgement

The authors would like to express sincere thanks for the financial supports by the National Natural Science Foundation (21103058, 21173091, 20903030), 973 Program of China (2011CBA00703), Natural Science Foundation of Hubei Province (2011CDB033, 2011CDB0.4) and Basic Scientific Research Funds for Central Colleges (2012YQ027, 2013TS040). We also thank Analytical and Testing Center of Huazhong University Science & Technology for the sample measurements.

Notes and references

[a] *Michael Grätzel Centre for Mesoscopic Solar Cells, Wuhan National Laboratory for Optoelectronics and College of Optoelectronic Science and Engineering, Huazhong University of Science and Technology, Wuhan 430074, P. R. China. Fax: 86 27 8779 3867; Tel: 86 27 8779 3867; E-mail: wnlochenwei@mail.hust.edu.cn* (Prof. W Chen), mingkui.wang@mail.hust.edu.cn (Prof. MK Wang)
[b] *Department of Materials Engineering, Monash University, Melbourne, Victoria, 3800, Australia*

1 F. Odobel, L.Le Pleux, Y. Pellegrin and E. Blart, *Acc. Chem. Res.*, 2010, **43**, 1063.
1. B. O'regan, M. Grätzel, *Nature* **1991**, 353, 737.
2. M. Gratzel, *J. Photochem. Photobiol., C.* **2003**, *4*, 145.
3. B. E. Hardin, H. J. Snaith and M. D. McGehee, *Nat. Photonics* **2012**, *6*, 162.
4. M. Gratzel, *Acc. Chem. Res*. **2009**, *42*, 1788.
5. A. Hagfeldt, G. Boschloo, L. C. Sun, L. Kloo and H. Pettersson, *Chem. Rev*. **2010**, *110*, 6595.
6. A. Yella, H. w. Lee, H. N. Tsao, C. Yi, A. K. Chandiran, M. K. Nazeeruddin, E. W. G. Diau, C. Y. Yeh, S. M. Zakeeruddin and M. Grätzel, *Sicence* **2011**, *334*, 629.
7. N. Memarian, I. Concina, A. Braga, S. M. Rozati, A. Vomiero, G. Sberveglieri, *Angew. Chem. Int. Ed.* **2011**, *50*, 12321.
8. A. Nattestad, A. J. Mozer, M. K. R. Fischer, Y. B. Cheng, A. Mishra, P. Bäuerle and U. Bach, *Nat. Mater.* **2010**, *9*, 31.
9. S. Powar, T. Daeneke, T. M. Michelle, U. Bach, *Angew. Chem. Int. Ed.* **2013**, *53*, 602.
10. E. A. Gibson, A. L. Smeigh, L. L. Pleux, J. Fortage, G. Boschloo, E. Blart, Y. Pellegrin, F. Odobel, A. Hagfeldt, L. Hammarström, *Angewandte Chemie* **2009**, 121, 4466–4469..
11. F. Odobel, Y. Pellegrin, E. A. Gibson, A. Hagfeldt, A. L. Smeigh, L. Hammarström, *Coordination Chemistry Reviews* **2012**, 256, 2414.
12. Z. Huang, G. Natu, Z. Ji, M. He, M. Yu, Y. Wu, *J. Phys. Chem. C* **2012**, 116, 26239.
13. J. Bandara, J. P. Yasomanee, *Semicond. Sci. Technol*. **2007**, 22, 20.
14. A. Nattestad, X. L. Zhang, U. Bach, Y. B. Cheng, *J. Photonics Energy* **2011**, 1, 011103.
15. M. Z. Yu, G. Natu, Z. Q. Ji and Y. Y. Wu, *J. Phys. Chem. Lett.* **2012**, 3, 1074.
16. A. Renaud, B. Chavillon, L. Le Pleux, Y. Pellegrin, E. Blart, M. Boujtita, T. Pauporté, L. Cario, S. Jobic and F. Odobel, *J. Mater. Chem*. **2012**, 22, 14353.
17. D. Xiong, Z. Xu, X. Zeng, W. Zhang, W. Chen, X. Xu, M. Wang, Y-B. Cheng, *J. Mater. Chem*. **2012**, 22, 24760.
18. D. Xiong, W. Zhang, X. Zeng, Z. Xu, W. Chen, J. Cui, M. Wang, L. Sun, Y-B. Cheng, *ChemSusChem*. **2013**, DOI: 10. 1002/cssc. 201300265.
19. H. Kawazoe, M. Yasukawa, H. Hyodo, M. Kurita, H. Yanagi, H. Hosono, *Nature* **1997**, 389, 939.
20. M. A. Marquardt, N. A. Ashmore, D. P. Cann, *The Solid Films* **2006**, 496, 146.
21. D. O. Scanlon, G. W. Watson, *J. Mater. Chem*. **2011**, 21, 3655.
22. R. Srinivasan, B. Chavillon, C. Doussier-Brochard, L. Cario, M. Paris, E. Gautron, P. Deniard, S. Jobic, *J. Mater. Chem*. **2008**, 18, 5647.
23. J. Yu, J. Fan, K. Lv, *Nanoscale*, **2010**, 2, 2144.
24. Y. Qiu, W. Chen, S. Yang, *Angewandte Chemie* **2010**, 122, 3757.
25. C. J. Barbé, F. Arendse, P. Comte, M. Jirousek, F. Lenzmann, V. Shklover, M. Grätzel, *Journal of the American Ceramic Society* **1997**, 80, 3157.
26. T. Yamaguchi, N. Tobe, D. Matsumoto, T. Nagai, H. Arakawa, *Solar Energy Materials and Solar Cells* **2010**, 94, 812.
27. Y. C. Qiu, W. Chen, S. H. Yang, *J. Mater. Chem*. **2010**, 20, 1001.
28. W. Chen, H. F. Zhang, I. M. Hsing, S. H. Yang, *Electrochem. Commun*. **2009**, 11, 1057.
29. W. Chen, Y. C. Qiu, Y. C. Zhong, K. S. Wong, S. H. Yang, *J. Phys.*

Chem. A **2010**, 114, 3127.
30. J. Halme, G. Boschloo, A. Hagfeldt, P. Lund, *J. Phys. Chem. C* **2008**, 112, 5623.
31. J. Tate, M. K. Jayaraj, A. D. Draeseke, T. Ulbrich, A. W. Sleight, K. A. Vanaja, R. Nagarajan, J. F. Wager, R. L. Hoffman, *Thin Solid Films* **2002**, 411, 119.

Graphical and textual abstract

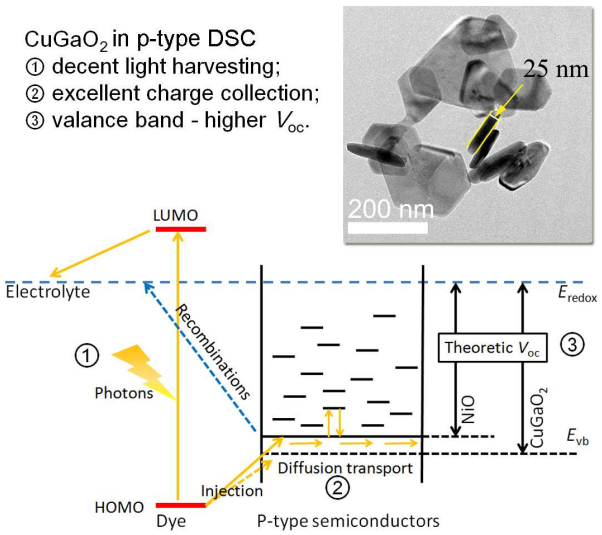

This work has demonstrate $CuGaO_2$ as efficient alternative to NiO as photocathode material in dye-sensitized solar cell. Deeper valance band position results in higher photovoltage. Critical size control of $CuGaO_2$ nanoplates and suitable film deposition technique lead to much enhanced light harvesting, in combination with excellent hole collection property, remarkable photocurrent has been achieved by $CuGaO_2$ photocathode.